ADVANCES IN ATMOSPHERIC SCIENCES, VOL. 34, NOVEMBER 2017, 1265–1281

• **Original Paper** •

A New Infrared Atmospheric Sounding Interferometer Channel Selection and Assessment of Its Impact on Met Office NWP Forecasts

Young-Chan NOH[1], Byung-Ju SOHN*[1], Yoonjae KIM[2], Sangwon JOO[2], William BELL[3], and Roger SAUNDERS[3]

[1]*School of Earth and Environmental Sciences, Seoul National University, Seoul* 08826*, Korea*
[2]*Numerical Modeling Center, Korea Meteorological Administration, Seoul* 07062*, Korea*
[3]*Met Office, Exeter EX*1 3*PB, United Kingdom*

(Received 2 December 2016; revised 4 May 2017; accepted 22 May 2017)

ABSTRACT

A new set of Infrared Atmospheric Sounding Interferometer (IASI) channels was re-selected from 314 EUMETSAT channels. In selecting channels, we calculated the impact of the individually added channel on the improvement in the analysis outputs from a one-dimensional variational analysis (1D-Var) for the Unified Model (UM) data assimilation system at the Met Office, using the channel score index (CSI) as a figure of merit. Then, 200 channels were selected in order by counting each individual channel's CSI contribution. Compared with the operationally used 183 channels for the UM at the Met Office, the new set shares 149 channels, while the other 51 channels are new. Also examined is the selection from the entropy reduction method with the same 1D-Var approach. Results suggest that channel selection can be made in a more objective fashion using the proposed CSI method. This is because the most important channels can be selected across the whole IASI observation spectrum.

In the experimental trial runs using the UM global assimilation system, the new channels had an overall neutral impact in terms of improvement in forecasts, as compared with results from the operational channels. However, upper-tropospheric moist biases shown in the control run with operational channels were significantly reduced in the experimental trial with the newly selected channels. The reduction of moist biases was mainly due to the additional water vapor channels, which are sensitive to the upper-tropospheric water vapor.

Key words: Hyperspectral IR sounding, channel selection, 1D-Var, data assimilation

Citation: Noh, Y.-C., B.-J. Sohn, Y. Kim, S. Joo, W. Bell, and R. Saunders, 2017: A new Infrared Atmospheric Sounding Interferometer channel selection and assessment of its impact on Met Office NWP forecasts. *Adv. Atmos. Sci.*, **34**(11), 1265–1281, https://doi.org/10.1007/s00376-017-6299-8.

1. Introduction

With the advent of satellite measurements and the development of data assimilation techniques, the impact of satellite observations in numerical weather forecasts has substantially increased in the last three decades. Bauer et al. (2015) showed that the three-day European Centre for Medium-Range Weather Forecasts (ECMWF) forecast skill, based on the 500-hPa height anomaly correlation in the Northern Hemisphere, has evolved from around 85% to 98% over the last three decades. The forecasting skill in the Southern Hemisphere, which was much lower than in the Northern Hemisphere three decades ago, is now as good as in the Northern Hemisphere. This reduction in the gap in the forecast skill between the hemispheres manifests the importance of better satellite observations in spectrum, space and time, and the assimilation scheme to optimally combine the observations and the forecasts. With the impressive improvement in satellite observations and assimilation schemes, satellite-measured radiances have become the most important observations for weather forecasting (English et al., 2000; Kelly and Thépaut, 2007; Dee et al., 2011; Lorenc and Marriott, 2014).

Among many different types of satellite data, high-spectral infrared sounder measurements are particularly interesting because high-spectral measurements contain rich information on the vertical structure of atmospheric temperature and water vapor. Indeed, such sounder measurements have had a considerable impact on weather forecasting at the UK Met Office (UKMO) (Hilton et al., 2009; Joo et al., 2013). Here, we focus on measurements from the Infrared Atmospheric Sounding Interferometer (IASI) instrument onboard the European Organisation for the Exploitation of Me-

* Corresponding author: Byung-Ju SOHN
Email: sohn@snu.ac.kr

teorological Satellites (EUMETSAT) MetOp satellites. The IASI instrument senses the emitted radiances in 8461 channels over the infrared spectral range of 645–2760 cm^{-1} (15.5–3.6 μm) at a resolution of 0.5 cm^{-1}, providing information on atmospheric temperature, humidity, cloud variables, and other trace gases. The instrument's field of view comprises a 2×2 array of circular pixels of 0.8° angular diameter (about 12 km at nadir) (Siméoni et al., 1997).

It may be desirable to use all of 8461 IASI channels during data assimilation if measurement errors are within the user-required preset values. However, the direct radiance assimilation of all IASI channels may be practically impossible due to the high data volume and heavy computational burden (Rabier et al., 2002; Collard, 2007). Furthermore, the current data transmission system operated by EUMETSAT may not disseminate all IASI channel data due to the data transmission costs. Instead, only a small subset of the whole channel data is distributed by EUMETSAT via the Global Telecommunication System for operational use at numerical weather prediction (NWP) centers.

Thus, channel selection is much desired, because a small subset should contain as much meteorological information as the whole 8461 channels, while substantially reducing the computational burden and data transmission cost. A total of 300 channels were selected by Collard (2007) and, based on this selection, a 314-EUMETSAT-channel dataset is operationally transmitted, including data from 14 monitoring channels at the Centre National d'Etudes Spatiales (CNES). In the operational Unified Model (UM) system, 183 of the 314 EUMETSAT channels are used in the observation processing system (OPS) for quality-control. However, only 138 channels have been assimilated into the NWP model because of technical problems associated with the UM system at the time when the IASI data were first introduced in 2007 (Weston, 2011). With an improved model and advanced radiative transfer modeling in the assimilation system after this first use, the technical problems met in the first attempt to select IASI channels may be alleviated. Nevertheless, there have been no attempts to add different channels or evaluate each channel's contribution in the current advanced assimilation system of the UM. Thus, in this study, we attempt to select new channels from the 314 EUMETSAT channels, which can replace the current 183 channels for better assimilation results.

Rabier et al. (2002) reviewed various channel selection methods for the high-spectral infrared sounder and concluded that Rodgers (2000) is the most optimal method. In fact, Collard (2007) used the Rodgers (2000) method for his selection of 300 channels. In Collard (2007), selection was made in each important spectral band, such as the CO_2, O_3, and H_2O absorption bands. This was because the degrees of freedom for the signal (DFS) and the entropy reduction (ER) in Rodgers (2000) were heavily influenced by water vapor channels (especially upper-tropospheric water vapor channels). But, because of there being no objective way to evaluate the relative merit of each band, a total of 300 channels were subjectively/evenly chosen by adding them all, after selecting channels in each absorption band. Thus, it is of interest to develop an objective way to evaluate the merit of each channel across the entire infrared spectrum.

In this study, we devise a way to select channels with the aid of a one-dimensional variational analysis (1D-Var), which can be used to select channels more objectively. The main aims are to reduce the problems caused by subjective or empirical decisions on channel selection. Details of the method are introduced in section 2. The Rodgers (2000) selection method adopted by Collard (2007) adopts fixed Jacobians, while the 1D-Var method devised in this study employs Jacobians variable with 1D-Var iterations. Thus, it is interesting to examine how the Rodgers (2000) method behaves if various Jacobians (resulting from the use of the 1D-Var approach) are applied. Thus, results from the Rodgers (2000) approach with various Jacobians will be compared with results from the proposed 1D-Var method.

In order to examine how the new IASI channels selected in this study improve the forecasting accuracy, in comparison to the current use of 183 channels in the operational UM data assimilation, we conducted trial experiments with two different sets of IASI channels. In these experiments, however, different from Observing System Simulation Experiment studies, all the same observations were kept as inputs to the system except the IASI observations. The results obtained in this study are expected to enhance our understanding of how channel selection can be made for extracting the most out of IASI observations, and thus improve our level of forecasting capability.

The channel selection methodology is introduced in section 2, and the characteristics of the newly selected channels are presented in section 3. In section 4, a comparison of different channel selection methods is provided. The impact of the new IASI channels on the UM global forecast is presented in section 5, followed by conclusions and discussion in section 6.

2. IASI channel selection methodology

Here, we describe how the methodology of IASI channel selection was developed in this study. Because the information on key atmospheric variables provided by channels can change under certain atmospheric conditions (e.g., overcast conditions), the selected channels may also change (Migliorini, 2015). In this study, we attempt to select IASI channels under clear-sky oceanic conditions.

2.1. *1D-Var*

The IASI channel selection is carried out after quantifying the degree of improvement in atmospheric variables retrieved from 1D-Var. In this procedure, 1D-Var minimizes the cost function $J(\boldsymbol{x})$ given as follows:

$$J(\boldsymbol{x}) = \frac{1}{2}(\boldsymbol{x}-\boldsymbol{x}_\mathrm{b})^\mathrm{T}\boldsymbol{B}^{-1}(\boldsymbol{x}-\boldsymbol{x}_\mathrm{b}) + \frac{1}{2}[\boldsymbol{y}_\mathrm{o}-H(\boldsymbol{x})]^\mathrm{T}\boldsymbol{R}^{-1}[\boldsymbol{y}_\mathrm{o}-H(\boldsymbol{x})], \tag{1}$$

where $\boldsymbol{x}$ is the control variable consisting of atmospheric variables, $\boldsymbol{x}_\mathrm{b}$ is the background variable, and $\boldsymbol{y}_\mathrm{o}$ is the observed

radiance in the given sensor channels. $\boldsymbol{B}$ is the background-error covariance matrix associated with the background variable $\boldsymbol{x}_\mathrm{b}$. $\boldsymbol{R}$ is the observation-error covariance matrix constructed from available error sources, including forward model errors, instrumental errors, errors from the different representativeness between observation and model, and systematic errors associated with the quality control. The superscript "T" indicates the matrix transpose and $H(\boldsymbol{x})$ is the forward-modeled radiance associated with the control variable $\boldsymbol{x}$. We attempt to find an analysis profile satisfying the minimum of the cost function (Rodgers, 2000; Deblonde et al., 2007; Pavelin et al., 2008).

2.2. *Simulation of IASI brightness temperature and background profile*

In order to perform 1D-Var retrievals, observed radiances for the selected IASI channels and background atmospheric variables are required as input data. Because this study quantitatively assesses the impact of inclusion of each of the preselected 314 IASI channels in terms of the degree of improvement in control variables obtained from 1D-Var, it is necessary to validate the 1D-Var outputs of temperature and humidity profiles against collocated in-situ measurements, such as radiosonde data. However, the assessment of the improved performance of the IASI channels used in the 1D-Var retrievals assumes that the true atmospheric conditions are known. The observed satellite radiances and background data are then theoretically generated with the given true atmospheric conditions.

For reference, we use a set of 600 profiles, which were randomly selected under clear-sky oceanic conditions from the ECMWF interim reanalysis (ERA-Interim) data in the year 2012. The reference data comprise temperature and moisture profiles at 37 standard pressure levels, surface pressure, surface humidity, and skin temperature. From these data, the IASI infrared brightness temperatures and background profiles are obtained and used as input data for the 1D-Var analysis in the NWP SAF (NWP satellite application facility) 1D-Var package version 3.4 (Weston et al., 2013).

For the IASI brightness temperature simulation, we use the Radiative Transfer for TIROS Operational Vertical Sounder (RTTOV) model, version 10, a fast radiative transfer model for data assimilation and retrieval systems (Matricardi et al., 2004). After interpolating temperature and water vapor profiles of the reference data to the required 43 standard pressure levels for RTTOV, IASI brightness temperatures in the preselected 314 channels [the 300 from Collard (2007) plus 14 monitoring channels] are simulated with clear-sky oceanic conditions. Forty-three levels are chosen because the UM 1D-Var uses the same 43 levels. In this simulation, random measurement errors are added to the simulated brightness temperatures, which are derived from the IASI observation-error covariance matrix used for the operational data assimilation system of the UM. Thus, observation errors in this simulation are thought to satisfy an unbiased Gaussian distribution and a diagonal observation-error covariance matrix is employed, implying that observation errors between any two IASI channels are assumed to be uncorrelated. However, the use of the diagonal observation-error covariance matrix may be problematic because of correlations existing between different channels (Bormann and Bauer, 2010; Weston et al., 2014). These correlations may arise from a variety of sources, such as instrument noise errors, forward model errors, representativeness errors, and systematic errors related to the pre-processing. The biggest contributions are from representativeness errors and systematic errors. Nevertheless, considering that theoretically-generated observations and background data in this study are independent of the scale mismatch between the observation and model, the representativeness errors caused by the mismatch can be ignored. The systematic errors can be ignored as well, because we use simulated radiances not requiring the quality-control step. On the other hand, observation-error correlations between neighboring channels caused by apodization were already considered because the 300 channels of Collard (2007) were selected by removing the nearest neighboring channels. However, two channels (689.50 cm^{-1} and 705.25 cm^{-1}) among the 14 CNES monitoring channels are next to Collard channels (689.75 cm^{-1} and 705.50 cm^{-1}), respectively. Nevertheless, the error correlation between CNES channels and neighboring Collard channels can be ignored, because random observation errors derived from the diagonal observation-error covariance matrix were added to the simulated IASI brightness temperatures. Therefore, it is reasonable to employ the diagonal observation-error covariance matrix with instrument noise errors so that IASI simulated radiances are suitably weighted against the background for 1D-Var.

Background estimates of the atmospheric state are also required for the 1D-Var simulation. In the operational assimilation system of the UM, 6-h forecasts from the previous data assimilation cycle are used as a background. However, in our work, the background is generated by adding random forecast errors to the reference data. The random forecast errors are calculated from the IASI background-error covariance used by the operational UM system. The background-error covariance matrix consists of the error covariance between 73 atmospheric and surface parameters (i.e., temperature at 43 pressure levels from 1013.25–0.1 hPa, water vapor at 26 pressure levels from 1013.25–122 hPa, surface temperature, surface humidity, skin temperature, and surface pressure). The forecast errors are then expressed by:

$$\boldsymbol{x}_0 = \boldsymbol{x}_\mathrm{t} + \sum_i \varepsilon_i \lambda_i^{\frac{1}{2}} \boldsymbol{E}_i \,, \tag{2}$$

where $\boldsymbol{x}_0$ is the perturbed background profile, $\boldsymbol{x}_\mathrm{t}$ is the reference profile, $\boldsymbol{E}_i$ and λ_i are the eigenvector and eigenvalue of the background-error covariance matrix, respectively, and ε_i is a random number with a zero mean and a unit standard deviation (Pavelin et al., 2008). For this work, we adopted the operationally used background-error covariance matrix, which is derived from the so-called National Meteorological Center (NMC) method (Parrish and Derber, 1992; English, 1999).

2.3. *Method for evaluating the impact of IASI channels*

The pre-defined information content, such as the DFS and the ER, which were employed in Collard (2007), is calculated using the full error-covariance matrices of both the background and analysis, and they represent the degree of improvement in the analysis error covariance against the background error covariance. However, because full error covariance is required for estimating such information content, it is difficult to evaluate the direct impact of channels on the retrieved variables when 1D-Var is employed. Here, since we aim to select channels based upon the direct contribution to the accuracy of retrieved atmospheric variables using 1D-Var, the channel selection in this work is based on a statistical method involving the comparison of 1D-Var results with background data.

Since in this case the true values of the atmospheric parameter $\boldsymbol{x}_t$ are known, the root-mean-square errors (RMSEs) of the analysis and background profile can be defined as follows:

$$\mathrm{RMSE}_{\mathrm{a},i,j} = \sqrt{\frac{\sum_{k=1}^{M}(x_{\mathrm{a},i,j,k} - x_{\mathrm{t},j,k})^2}{M}}\,,$$
$$\mathrm{RMSE}_{\mathrm{b},j} = \sqrt{\frac{\sum_{k=1}^{M}(x_{\mathrm{b},j,k} - x_{\mathrm{t},j,k})^2}{M}}\,. \tag{3}$$

In Eq. (3), the subscript i denotes the IASI channel number (i.e., $i = 1,2\ldots314$) used; the subscript j denotes the atmospheric and surface parameter number (i.e., $j = 1,2\ldots43$ for temperature at 43 pressure levels from 1013.25 to 0.1 hPa, $j = 44,45\ldots69$ for water vapor at 26 pressure levels from 1013.25 to 122 hPa, and $j = 70,71\ldots73$ for surface 2-m temperature, surface 2-m humidity, skin temperature, and surface pressure); and the subscript k denotes an index for the 600 reference profiles (i.e., $M = 600$, $k = 1,2\ldots M$). The subscripts a, b, and t represent the analysis, background, and true reference profile, respectively. Thus, $\mathrm{RMSE}_{\mathrm{a},i,j}$ is the RMSE between the analysis and reference for the jth analysis parameter, for an i number of IASI channels selected for 1D-Var. $\mathrm{RMSE}_{\mathrm{b},j}$ is the RMSE between the background and reference for the jth parameter. To select the total number of i channels out of the 314 provisional channels, instead of random selection, we devised an efficient method, described in section 2.4.

In order to assess the overall impact of a particular set of selected IASI channels on the improvement in the analysis parameters for 1D-Var, the following channel score index (CSI) is defined as a figure of merit:

$$\mathrm{CSI} = \sum_{j=1}^{N}\left(1 - \frac{\mathrm{RMSE}_{\mathrm{a},i,j}}{\mathrm{RMSE}_{\mathrm{b},j}}\right)w_j\,, \tag{4}$$

where w_j is the weight associated with the jth atmospheric parameter, and N is the total number of atmospheric parameters used for calculating the CSI (i.e., $N = 73$). The CSI value indicates the degree of improvement in the analysis profile over the background profile. A positive CSI means that the analysis error is smaller than that of the background, implying that the selected IASI channels for the 1D-Var analysis are contributing positively.

Concerning w_j for water vapor in Eq. (4), it is noted that the contribution of upper-tropospheric water vapor to the CSI tends to be comparatively large and highly variable despite small amounts of water vapor (not shown). In order to show the water vapor background error varying with height, the background error normalized by the level's mean value is plotted in Fig. 1a. The normalized error becomes close to the

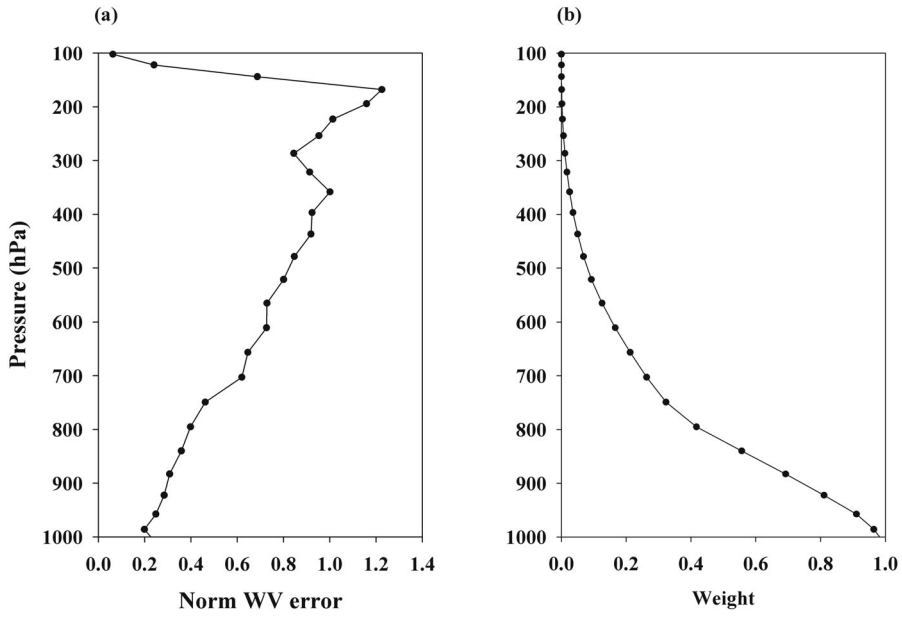

Fig. 1. The (a) normalized background water vapor error against the mean water vapor mixing ratio (kg kg^{-1}) and (b) vertical structure of the weight applied to the water vapor contribution to the channel score index (CSI).

level's value itself above the 400 hPa level. Because of the larger error percentage in the upper layers, any small RMSE improvement in the upper layer contributes to the CSI with a much larger ratio, compared with the same RMSE improvement in the lower layers. Therefore, it is necessary to apply weights to the water vapor contribution to the CSI, in order to alleviate the comparatively large influence from the upper-tropospheric water vapor. The weight for the water vapor at each level is obtained by using the mean profile obtained from 600 samples of profiles; the weight at a particular level is estimated by normalizing the mean water vapor mixing ratio at that level with the mean water vapor at the lowest level (Fig. 1b). The weights (for the 44th to 69th water vapor parameters), at 26 pressure levels, decrease gradually from 1 at the surface to a much smaller value at the top level of 122 hPa. The weights for other atmospheric parameters are set to 1.

2.4. *Channel selection*

First, the CSI is calculated for each of the provisional 314 IASI channels, in order to find the channel that has the largest contribution to the CSI. Then, that channel is considered to be the first selected channel. Second, each of the remaining 313 channels is added to the first selected channel (forming two channels) so that the impact of the two selected channels on the CSI can be estimated. The channel that gives the largest contribution to the CSI after it is combined with the first selected channel is considered to be the second selected channel. The third channel is selected by determining which channel of the remaining 312 channels gives the largest contribution to the CSI when added to the first two selected channels. This procedure is repeated until the last channel is left.

3. Characteristics of the newly selected IASI channels

Figure 2 shows the CSI calculated from the 1D-Var simulation with the selected channels by applying the procedures described in section 2. It is shown that the CSI increases rapidly with an increasing number of selected channels, reaching up to 85% of the total CSI at 60 selected channels and 93% at 100. The slope tends to decrease slowly after 100 selected channels, and the CSI approaches an asymptotic value, especially when the number of selected channels becomes close to 200. After 200 selected channels, additional channels have little impact on the CSI, suggesting that the first 200 channels contain most of the information required for improving the background atmospheric state. Furthermore, there is a tendency for less convergence in 1D-Var when more than 200 channels are used. Considering that IASI observations causing convergence failure in 1D-Var should be discarded before further use for the data assimilation, the first 200 channels yielding most of the CSI could be considered optimal for the IASI data assimilation for atmospheric temperature and water vapor retrievals.

It can also be seen that the selected 200 channels are distributed largely over the CO_2 (650–750 cm^{-1}), H_2O (1350–2000 cm^{-1}), and O_3 (1030 cm^{-1}) absorption bands in the IASI spectrum from 645–2760 cm^{-1} (Fig. 3). Most of the channels over the CO_2 absorption band recommended by Collard (2007) were selected in this new selection (Fig. 3b). Selected H_2O channels seem to be divided into two groups: one near 2000 cm^{-1} and the other over a 1300–1600 cm^{-1} band. Since the former carries the water vapor information over the lower troposphere and the latter over the mid to upper troposphere, H_2O channels near 1600 cm^{-1} that are sensitive to the upper-tropospheric water vapor are very rare. The fewer selected H_2O channels for the upper troposphere, in comparison to the near full selection of available CO_2 channels, are likely due to the larger instrumental noises of H_2O channels, which can cause a larger observation-error covariance. Instrumental noise errors for H_2O channels appear to be larger and more variable than those for CO_2 channels—see Fig. 2 of Collard (2007). Given the fact that the error covariance is closely related to the instrumental noise, H_2O channels are less capable of increasing the CSI and thus are selected less in comparison to the CO_2 channels. Besides the major selection of channels over CO_2 and H_2O absorption bands, selected channels are found over the 1030 cm^{-1} O_3 absorption band and in the split window channels over the 900 cm^{-1} and 1100 cm^{-1} spectral bands.

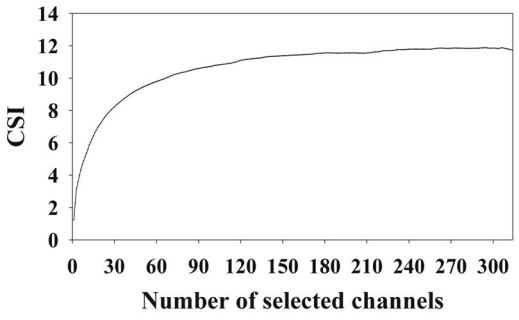

Fig. 2. Relationship between the CSI and the number of selected IASI channels.

It is of interest to examine how the 200 newly selected channels are different from the 183 IASI channels, which have been used operationally in the UM global forecast system at the UKMO since the year 2007 (Weston, 2011). This is of interest because the UM model has been improved since the IASI data were first used.

It is found that 149 out of the operationally used 183 channels are also shown in the new 200 channels (Fig. 4a), and thus 34 channels (Fig. 4b) are not included in the 200 channels. Fifty-one channels selected only from the 200 new channels (Fig. 4c) are located mainly in the O_3 band over 1030 cm^{-1}, the H_2O bands around 1350 cm^{-1} and 2000 cm^{-1}, and in band 3 (2000–2760 cm^{-1}). From the comparison of the weighting functions between the newly selected 200 channels and the operational 183 channels, the vertical distributions of weighting functions for new channels are found to be more evenly distributed (not shown). It seems this is due to the addition of more middle- and upper-tropospheric

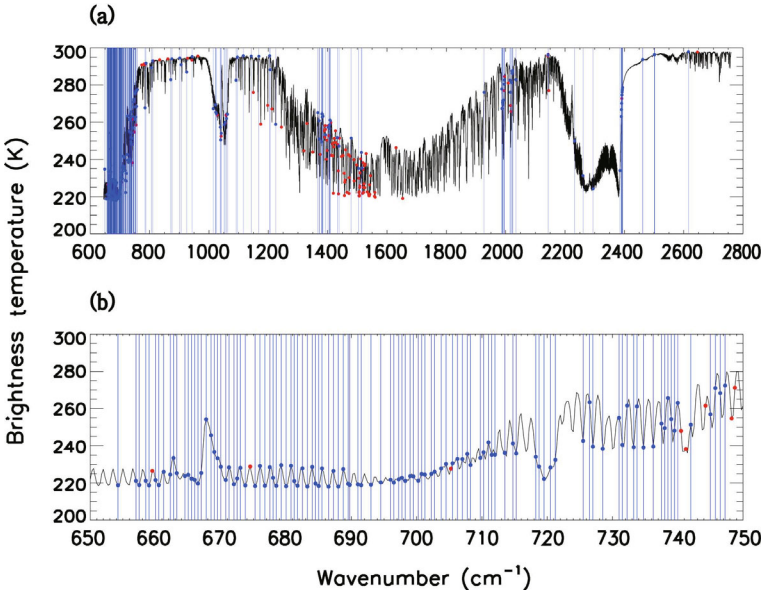

Fig. 3. Spectral distributions (black line) of the 200 newly selected IASI channels over the (a) infrared band (600–2800 cm^{-1}) and (b) CO_2 absorption band (650–750 cm^{-1}). Blue bars and red dots indicate the 200 selected IASI channels and remaining 114 channels among the provisional 314 IASI channels, respectively.

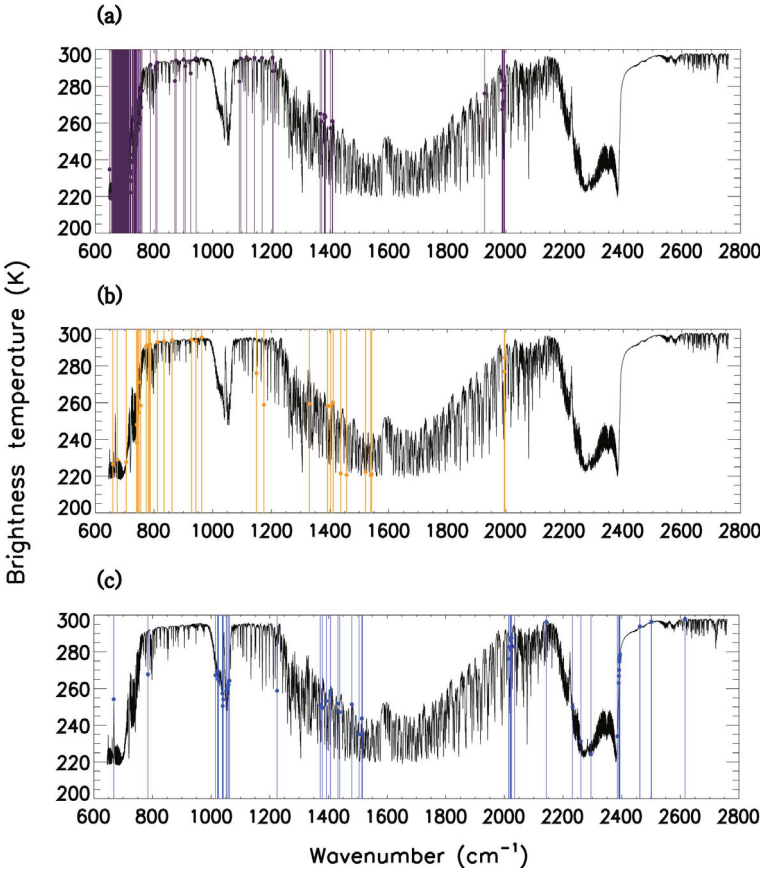

Fig. 4. Spectral distributions of the (a) 149 channels commonly shown in both the 183 operational channels and the 200 new channels, (b) 34 operationally used channels excluded from the 200 new channels, and (c) 51 new channels excluded from the 183 operational channels. Vertical lines and dots in color indicate the spectral positions of channels.

channels while removing surface-sensitive channels.

It is not surprising to find channels over the O_3 band because the UM OPS noted that the use of O_3 channels in the IASI data assimilation in 2007 could cause a divergence during the 1D-Var minimization process. High-peaking H_2O channels (1300–1600 cm^{-1}) whose temperature Jacobian peaks are located above 520 hPa were also removed because of the same minimization problem (Hilton et al., 2009). However, six high-peaking H_2O channels (corresponding to channel wave numbers 1436.75, 1456.75, 1521.25, 1539.0, 1540.25, and 1542.0 cm^{-1}) survived for the assimilation. These channels have Jacobians without well-defined peaks and with long tails into the stratosphere, but have a slightly positive influence on the forecasts (Smith, 2014). In our new H_2O channel selection, the channels that survived were replaced by other H_2O channels with high peaks above 520 hPa.

4. Comparison with the entropy reduction method

Since the CSI is estimated from errors of 1D-Var–retrieved and background atmospheric variables, it is interesting to examine how the use of full error covariance might influence the channel selection. In this part of our study, the ER method is employed, which can be estimated from the error-covariance matrix reflecting error correlations between atmospheric parameters at different levels (Rodgers, 2000), i.e.,

$$\mathrm{ER} = -\frac{1}{2}\ln[\det(\boldsymbol{A}\boldsymbol{B}^{-1})]\,, \tag{5}$$

where $\boldsymbol{A}$ and $\boldsymbol{B}$ indicate the analysis and background error covariance matrices. In this ER method, the selection procedures are the same as in the CSI approach, except for the use of ER. In order to select the optimal channels for a diverse range of atmospheric profiles, an ER mean is calculated from the same 600 atmospheric profiles used for the CSI approach:

$$\overline{(\mathrm{ER})}_i = \frac{\sum_j^M \left\{-\frac{1}{2}\ln[\det(\boldsymbol{A}_{i,j}\boldsymbol{B}^{-1})]\right\}}{M}\,, \tag{6}$$

where the subscript i denotes the channel number (i.e., $i = 1,2\ldots314$) used for the 1D-Var and the subscript j the index for 600 atmospheric profiles (i.e., $M = 600$, $j = 1,2\ldots M$). Thus, $\overline{(\mathrm{ER})}_i$ indicates an ER mean from i IASI channels used for 1D-Var.

Figure 5 shows the ER mean in selected IASI channels. Compared to the CSI results (Fig. 2), the ER increases rather slowly, reaching 82% in 100 and 90% in 170 selected channels—as compared with the CSI results of 93% in 100 and 96% in 170. Furthermore, the ER steadily increases even after 200, where the ER reaches about 94% of the total. These results suggest that the selected channels may be close to 314 when the ER method is used—far more channels than suggested by the CSI method.

The spectral distribution of the first 200 channels selected with the ER is given in Fig. 6 for comparison with the CSI results. Compared with the CSI results (Fig. 3a), the ER method selected fewer channels over the CO_2 absorption band, but more H_2O channels over 1350–2000 cm^{-1}. In particular, many more upper-tropospheric H_2O channels over 1350–1600 cm^{-1} were selected. The substantial difference in the two sets of selected channels suggests that each channel contributes differently to the two indices.

In order to examine how each channel contributes to the ER and the CSI, we estimate the ER and the CSI in each of the 314 provisional channels, and the results are given in Fig. 7. As expected, channels over the CO_2 (650–750 cm^{-1}) and H_2O (1350–2000 cm^{-1}) absorption bands, and the window

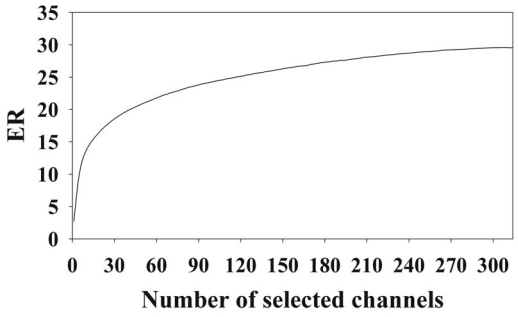

Fig. 5. Relationship between the Entropy reduction (ER) and the number of selected IASI channels.

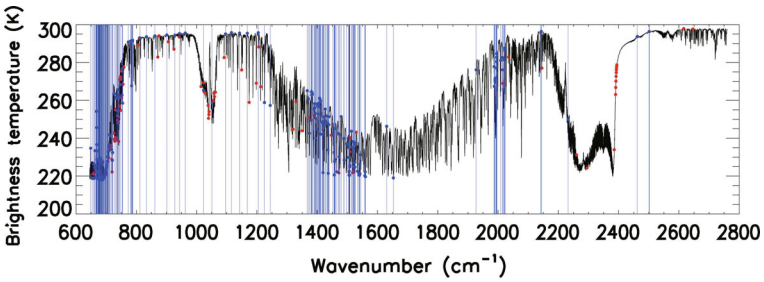

Fig. 6. Spectral distribution (black line) of the 200 IASI channels with ER over the infrared band (600–2800 cm^{-1}). Blue bars and red dots indicate the 200 selected IASI channels and remaining 114 channels among the provisional 314 IASI channels, respectively.

regions (900 cm^{-1} and 1100 cm^{-1} spectral bands), contribute to the ER through the improvement of temperature, water vapor, and surface variables, respectively (Fig. 7a). It is noted that contributions of water vapor to the ER for H_2O channels, particularly associated with upper-tropospheric humidity, are much stronger than for channels in any other spectral bands. This suggests that upper-tropospheric H_2O channels are selected first, prior to other channels, as shown in Fig. 6. Heavy contributions by water vapor in the ER approach may be alleviated if weights are given to water vapor profiles. However, it is difficult to give weights while counting all the correlations between levels. Therefore, even if the 1D-Var approach is adopted for the ER method, the procedures should be taken individually over separate absorption bands.

The CSI results given in Fig. 7b show similar features found from the ER (Fig. 7a). However, the contribution by water vapor to the CSI over the H_2O absorption band appears small due to the applied weights.

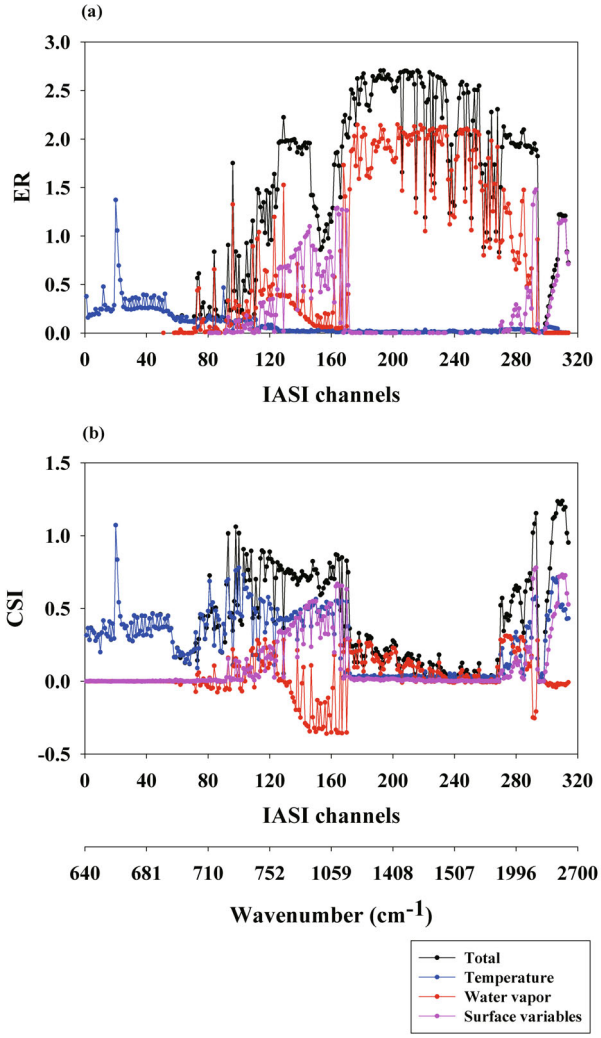

Fig. 7. Contribution of temperature (blue), water vapor (red), and surface variables (pink) to (a) the total entropy reduction ER and (b) the channel score index (CSI) for each of 314 IASI channels.

5. Impact of the new IASI channels on UM global forecasts

Global model assimilation trials were carried out for a period from 4 July to 7 August 2013, to examine the impact of the new set of IASI channels on the analysis fields of the operational assimilation system and resultant forecasts. The trials consisted of control and experiment runs. The 183 operational IASI channels were used in the control run and were replaced by the new 200 IASI channels in the experiment run. All the baseline observations were the same for both runs, which were performed with the operational global UM at the UKMO.

5.1. *Assessment of first-guess departure*

For assimilating the satellite observation data, a quality-control process known as OPS in the operational UM system is performed. Satellite-observed radiances are compared with the radiances simulated with collocated model-generated atmospheric fields (called the background) using a radiative transfer model (e.g., RTTOV). Background fields are the UM 6-h forecasts issued from the previous data assimilation cycle. Through examination of the departure of simulated radiances from satellite observations, the performance of the background fields can be monitored.

The experiments with the new 200 IASI channels had a substantially smaller data volume ratio of IASI observations passing through the OPS than the control run. This significantly reduced volume of IASI observations was due to O_3 channels included in the new 200 IASI channels. The use of climatological O_3 concentrations in the UM for the O_3 channel simulations caused larger departures from the observed radiances, resulting in a convergence failure in the 1D-Var process (e.g., Saunders et al., 2013). Thus, O_3 channels were excluded from the 200 IASI channels in the experiment runs, in order to increase the convergence ratio for 1D-Var in the OPS. This resulted in a selection of 189 channels, which is close to the operationally used 183 channels.

Similar problems may arise from the use of shortwave infrared channels over band 3 during the daytime because of solar contamination. Thus, the nighttime band 3 measurements were used, which were defined as those with a solar zenith angle greater than 95°.

In order to examine the impact of the new IASI channels on the background field, atmospheric profiles of the background from the control and experiment runs were used as inputs to RTTOV to simulate channel radiances of the Advanced TIROS Operational Vertical Sounder (ATOVS). The ATOVS consists of three instruments: the High Resolution Infrared Radiation Sounder (HIRS), the Advanced Microwave Sounding Unit-A (AMSU-A), and the Microwave Humidity Sounder (MHS). The differences in first-guess departure between the control and experiment runs for the ATOVS channels in four satellite platforms (i.e., MetOp-A, MetOp-B, NOAA-18, and NOAA-19) are shown in Fig. 8. The characteristics of ATOVS channels are given in Table 1. From the comparison between the control and experiment

Table 1. Characteristics of ATOVS channels used in the UM data assimilation.

Instrument	Channel	Channel index	Wavenumber (cm^{-1})	Wavelength (μm)	Principal absorber
HIRS	2	2	679	14.7	CO_2
HIRS	3	3	691	14.5	CO_2
HIRS	4	4	704	14.2	CO_2
HIRS	5	5	716	14.0	CO_2
HIRS	6	6	732	13.7	CO_2
HIRS	7	7	748	13.4	CO_2
HIRS	8	8	898	11.1	Window
HIRS	10	10	1217	8.3	H_2O
HIRS	11	11	1364	7.3	H_2O
HIRS	12	12	1484	6.7	H_2O
HIRS	13	13	2190	4.57	CO_2
HIRS	14	14	2213	4.52	CO_2
HIRS	15	15	2240	4.46	CO_2
Instrument	Channel	Channel index	Frequency (GHz)	Polarization angles	Principal absorber
AMSU-A	1	21	23.8	90–θ	Window
AMSU-A	2	22	31.4	90–θ	Window
AMSU-A	4	24	52.8	90–θ	O_2
AMSU-A	5	25	53.6	θ	O_2
AMSU-A	6	26	54.4	θ	O_2
AMSU-A	7	27	54.9	90–θ	O_2
AMSU-A	8	28	55.5	θ	O_2
AMSU-A	9	29	57.29	θ	O_2
AMSU-A	10	30	57.29 ± 0.217	θ	O_2
AMSU-A	11	31	$57.29 \pm 0.322 \pm 0.048$	θ	O_2
AMSU-A	12	32	$57.29 \pm 0.322 \pm 0.022$	θ	O_2
AMSU-A	13	33	$57.29 \pm 0.322 \pm 0.010$	θ	O_2
AMSU-A	14	34	$57.29 \pm 0.322 \pm 0.0045$	θ	O_2
MHS	3	38	183.31 ± 1.0	θ	H_2O
MHS	4	39	183.31 ± 3.0	θ	H_2O
MHS	5	40	190.31	90–θ	H_2O

runs, little difference was found in the temperature sounding channels of ATOVS (i.e., HIRS channels 2–7, given as channel indices of 2–7, and AMSU-A channels 1–14, given as channel indices of 21–34). By contrast, significant differences were noted in the H_2O channels (HIRS 12, given as channel index of 12, and MHS 3–4, given as 38–39). Considering that these H_2O channels show Jacobian peaks in the upper troposphere, the new channels may provide a bigger impact on the upper-tropospheric humidity field. However, considering the finding that negative biases become larger, especially for the upper-tropospheric channels (e.g., channel indices 12 and 38), the experiment run should induce a relatively drier upper troposphere in the 6-h forecast. The negative biases of the upper-tropospheric humidity channels were persistent throughout the analysis period. Persistent larger biases were also clear in the experiment run.

Such drier biases shown in the experiment run were also evident in the comparison with simulations for other infrared sensors [i.e., the Atmospheric Infrared Sounder (AIRS) and Cross-track Infrared Sounder (CrIS) hyperspectral sounders] with the same background fields. In the UM forecasting, 324 AIRS and 399 CrIS channels over the CO_2 and H_2O absorption bands, and the window region, are included in the system (Cameron et al., 2005; Gambacorta and Barnet, 2013). However, similar to the IASI channel selection, some of the AIRS and CrIS channels were not used for data assimilation—the unused channels are indicated as empty spaces in Fig. 9. The experiment run showed larger negative mean biases for H_2O channels (e.g., AIRS 174–235 and CrIS 185–312 channels), compared to the positive biases shown in the control run. In particular, the larger negative biases were located over higher channel numbers, which represent channels sensitive to the upper-tropospheric humidity. Such relative dry biases for the experiment run are consistent with the ATOVS results shown in Fig. 8.

As shown in the first-guess departures of the ATOVS, CrIS, and AIRS H_2O channels, the new IASI channel selection causes larger biases, and the larger biases suggest inferior performance in the assimilated water vapor field. However, considering that the biases between the satellite observations and model backgrounds are subtracted from satellite observations before use for data assimilation (called "bias correction"), the larger H_2O channel biases might be related to such bias correction.

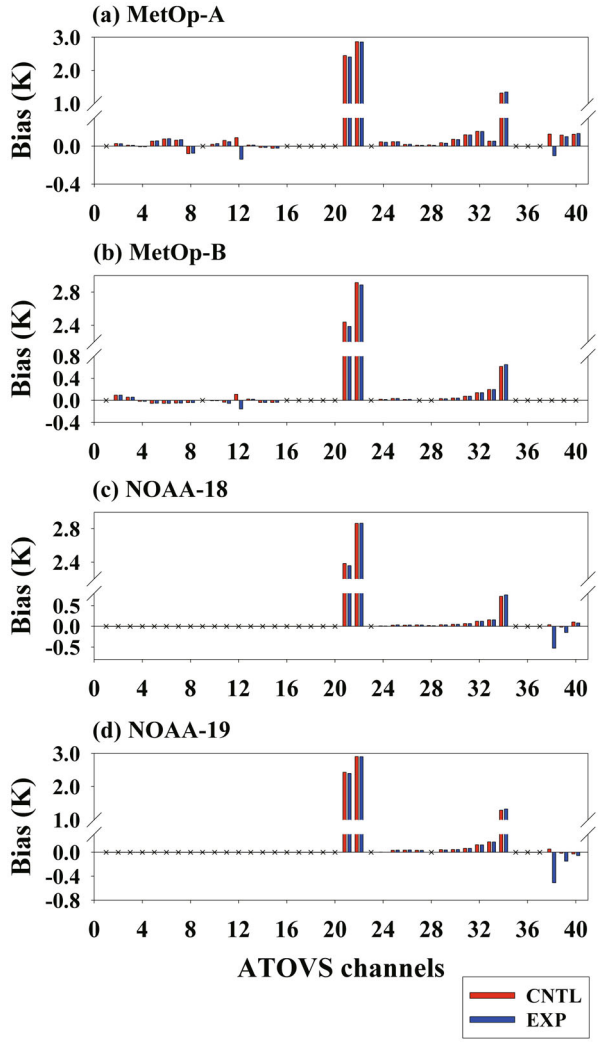

Fig. 8. Mean first-guess departures for ATOVS channels onboard the (a) MetOp-A, (b) MetOp-B, (c) NOAA-18, and (d) NOAA-19 satellites for the period from 4 July to 7 August 2013. The red and blue bars indicate results from the control (CNTL) and experiment (EXP) runs, respectively. Channel characteristics are shown in Table 1.

Here, for the bias correction, we use the correction scheme employed by the UM OPS, which is based on the bias correction scheme developed by Harris and Kelly (2001) for satellite measurements. The scheme uses the geometric thicknesses of the 850–300 hPa and 300–50 hPa layers in the model atmosphere as predictors to regress to the departures between IASI observations and background-derived radiances. Once regression coefficients and an intercept point are determined for each of all the 314 selected IASI channels, the biases for the 189 IASI channels used are predicted by inserting two layer thicknesses into the obtained regression equation. Since our main aim is to examine how the new set of channels improves the forecasts through the improvement of the background field, recalculation of bias correction coefficients for the current experiment may not be necessary and therefore the same bias correction coefficients were used for both the experiment and control runs.

The bias correction mostly removes biases related to instrument errors and uncertain radiative transfer modeling. These biases are variable with time because of sensor degradation or upgrading of the radiative transfer model. However, in the two trial runs (control and experiment run) in this study, the same satellite data were used along with the same version of radiative transfer model. Because sensor-related errors and systemic errors were the same for both runs, the same bias correction coefficients could be used for both runs.

Here, using radiosonde observations, we examine the abovementioned bias correction as a possible cause for the larger negative H_2O channel departures shown in Figs. 8 and 9. The mean biases of first-guess departures obtained from radiosonde observations in the assimilation cycle are shown in Fig. 10. Negative biases are clear for both the control and experiment runs, suggesting that the backgrounds (i.e., 6-h forecasts) are humid over almost the entire troposphere, as compared to radiosonde observations (Fig. 10). Much larger humidity biases of the control run over the upper troposphere are significantly different from the near-zero bias shown in the first-guess departures (Figs. 8 and 9), and this is thought to be due to the bias correction made in the OPS. For the

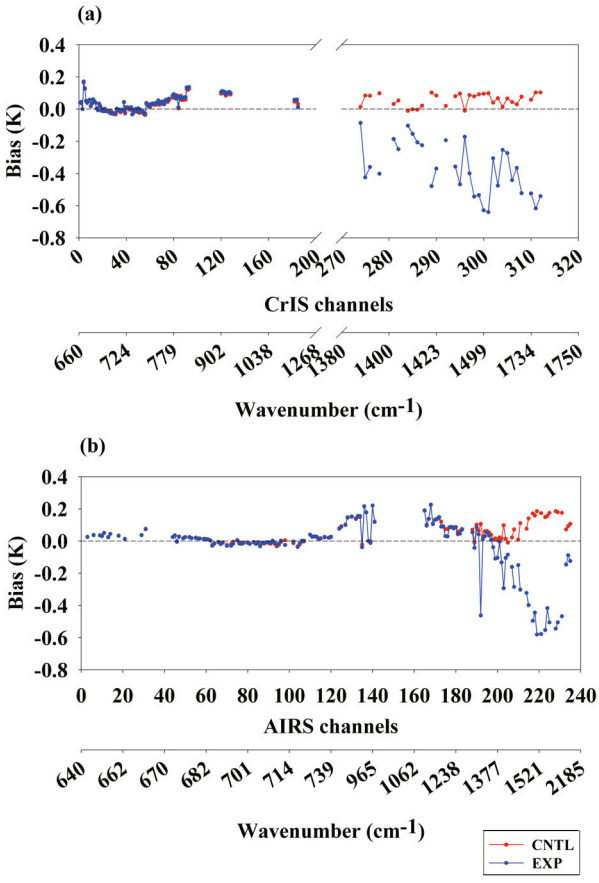

Fig. 9. Mean first-guess departures for (a) CrIS and (b) AIRS channels for the period from 4 July to 7 August 2013. The red and blue lines indicate the results from the control (CNTL) and experiment (EXP) runs, respectively.

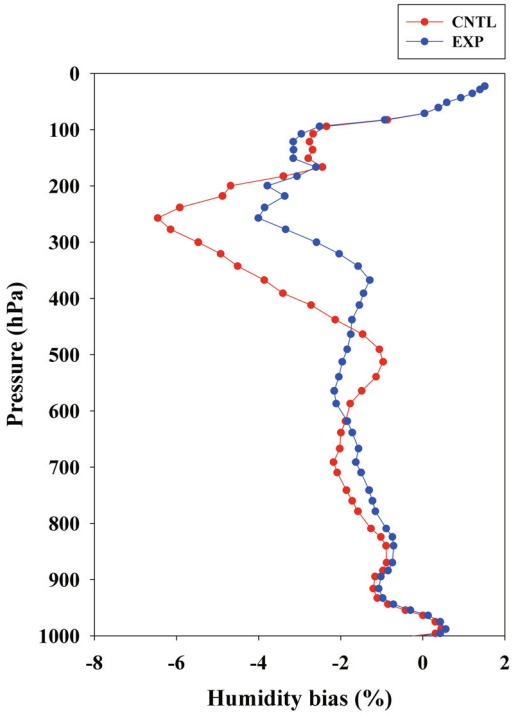

Fig. 10. Mean first-guess departures for radiosonde relative humidity profiles for the control (CNTL; red line) and experiment (EXP; blue line) runs.

satellite-measured radiance assimilation, biases are removed from the observations in order to make observations consistent with model backgrounds. Thus, the apparent near-zero biases of the H_2O channels in Figs. 8 and 9 do not necessarily mean a nearly unbiased moisture condition in the control run, as noted in the humid condition in Fig. 10. The bias correction in the control run should have been a positive brightness temperature subtraction from the satellite measurements (i.e., colder H_2O channel temperatures representing humid conditions). The experiment run, on the other hand, indicates a less humid condition in comparison to the control run (Fig. 10). Since the coefficients used in bias correction for both the experiment and control runs were the same, the apparent departures should be negative, as in Figs. 8 and 9, because of the less humid conditions as shown in Fig. 10. Thus, we conclude that the larger negative departures shown in the H_2O channels (Figs. 8 and 9) are due to the use of the same bias correction for both the control and experiment runs, and the near-zero biases in the control run should not mean an unbiased humidity condition.

5.2. *Impact assessment using global model assimilation trials*

In order to examine the impact of the new IASI channels on UM global forecasts, departures of forecast atmospheric parameters obtained from each trial run against radiosonde observations were calculated. The score, called the global NWP index, was used to measure the forecast impact in the UKMO UM system; it combines the scores of particular atmospheric parameters at each forecast hour. The total index is the sum of the scores from all the atmospheric parameters. Details regarding how to derive the scores are found in Appendix A of Rawlins et al. (2007).

The global NWP index calculated for the experiment shows that the newly selected IASI channels have an overall neutral impact on the forecast improvement for the selected atmospheric parameters, compared to the control run (not shown). Since the main difference between the new IASI channels and the currently used operational IASI channels is the use of different H_2O channels and band 3 channels, it is not surprising to find little improvement in the NWP index, based on parameters such as mean-sea-level pressure, 500 hPa geopotential, and winds at 250 hPa and 850 hPa.

In contrast, the forecast temperature and relative humidity parameters, which are not part of the NWP index calculation, show a significant improvement, especially above 500 hPa. Figures 11 and 12 show the mean biases of temperature and relative humidity at the 500 hPa and 850 hPa levels, in the range of T+0 to T+72 forecast hours. The mean biases of the forecast temperature at 500 hPa level were smaller for the experiment run, compared to those from the control run, in both the Northern and Southern Hemisphere, although the mean bias in the Southern Hemisphere at T+36 became larger first. In contrast, the forecast error for the temperature at 850 hPa shows a slight degradation for the experiment run.

In terms of humidity in the control and experiment runs, the positive biases of relative humidity at the 250 hPa level are significantly reduced by up to 4% in the experiment run in both hemispheres, as shown in Figs. 12a and b. However, for the mean bias difference at the 850 hPa level for temperature, the difference in relative humidity also shows a less significant impact. The RMSEs of relative humidity are slightly reduced at the 250 hPa level in the experiment run, but are quite similar at the 850 hPa level (Fig. 13). It is clear that the improvement in the relative humidity forecasts mainly occurred in the upper troposphere from 500 hPa to 200 hPa. A substantial bias reduction is evident in the analysis at T+0. By contrast, in the mid-troposphere from 600 hPa to 500 hPa, the mean biases are larger for the experiment run at T+0 and T+24 (Figs. 14a and b). The humidity RMSEs are mainly reduced in the upper troposphere from 350 hPa to 200 hPa at T+0 and T+24, but the RMSE reduction at T+48 and T+72 appears to be insignificant (Fig. 15). As expected, the humidity biases and RMSEs increase with the forecast hour in both runs, even though the mean biases and RMSEs in the experiment run are smaller than those in the control run.

Considering that the main difference between the new channels and the 183 UKMO operational channels lies in the use of the new IASI H_2O channels and band 3 channels, the improvement in the temperature and relative humidity forecasts in the upper troposphere can be attributed to the use of these new additional channels. Since weighting functions of the selected IASI band 3 channels are mostly located in the lower troposphere, we expect improved temperature forecasts in the lower troposphere. However, there is only a small change in the lower troposphere from the use of the new channels, which suggests that the impact of the band 3 channels

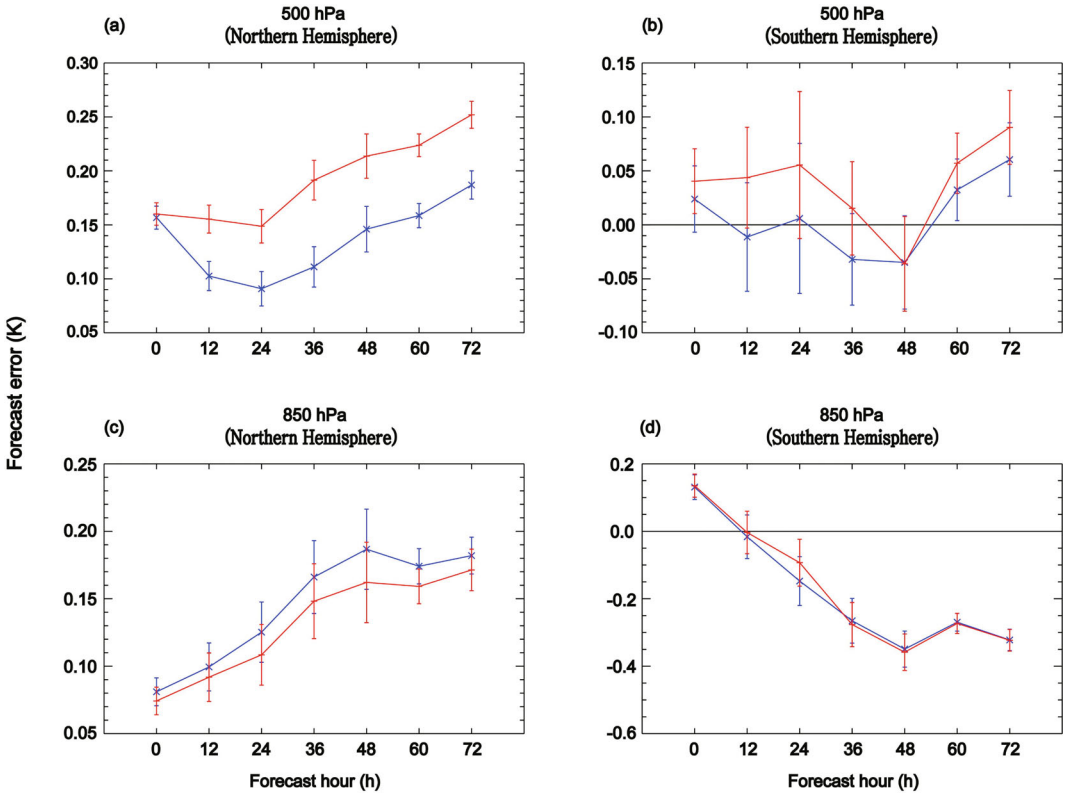

Fig. 11. Mean biases of (a, b) 500 hPa and (c, d) 850 hPa temperature forecast errors between forecasts and radiosonde observations over the (a, c) Northern and (b, d) Southern Hemisphere. Red and blue indicate the control and experiment runs, respectively. Vertical bars representing one standard deviation of the uncertainty are overlaid.

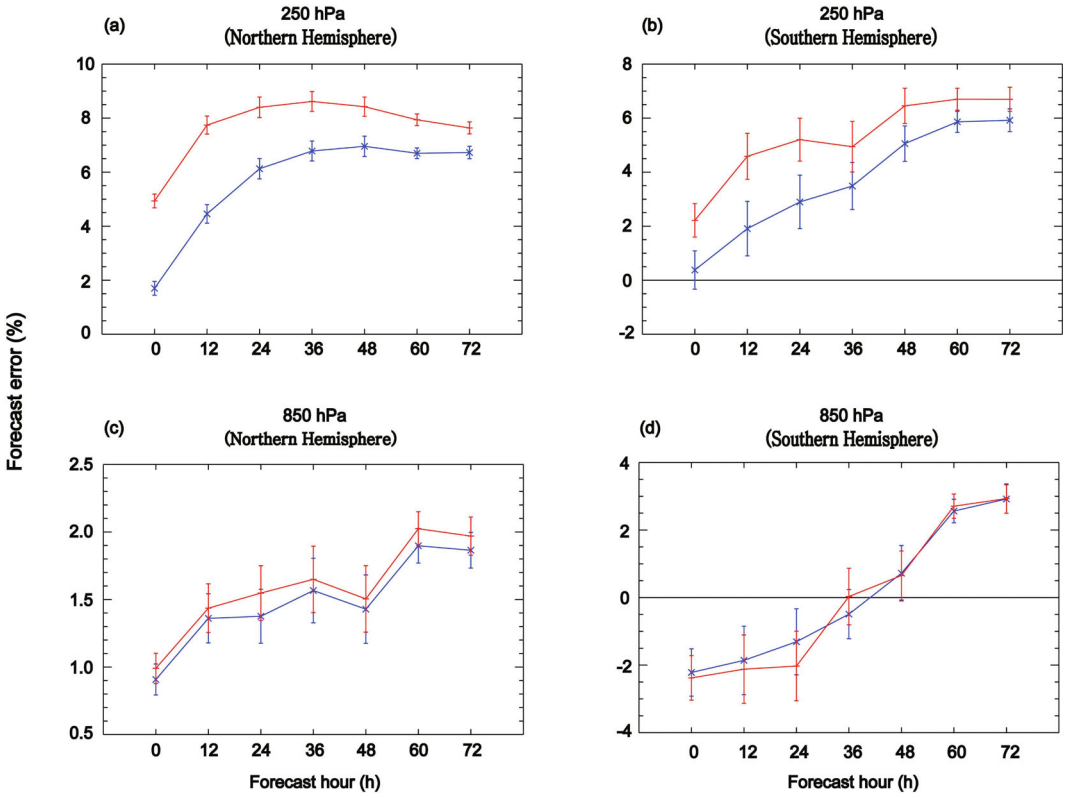

Fig. 12. As in Fig. 11 but for relative humidity forecast errors.

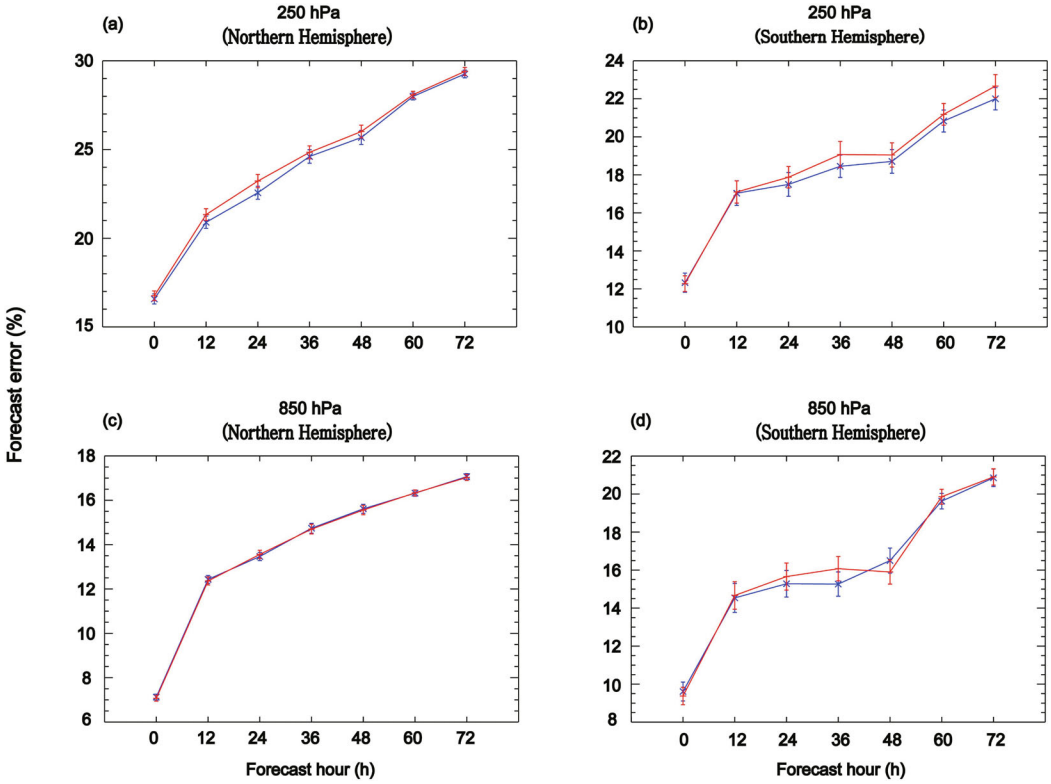

Fig. 13. The RMSE of (a, b) 250 hPa and (c, d) 850 hPa relative humidity forecast errors between forecasts and radiosonde observations over the (a, c) Northern and (b, d) Southern Hemisphere. Red and blue lines indicate the control and experiment runs, respectively. Vertical bars representing one standard deviation of the uncertainty are overlaid.

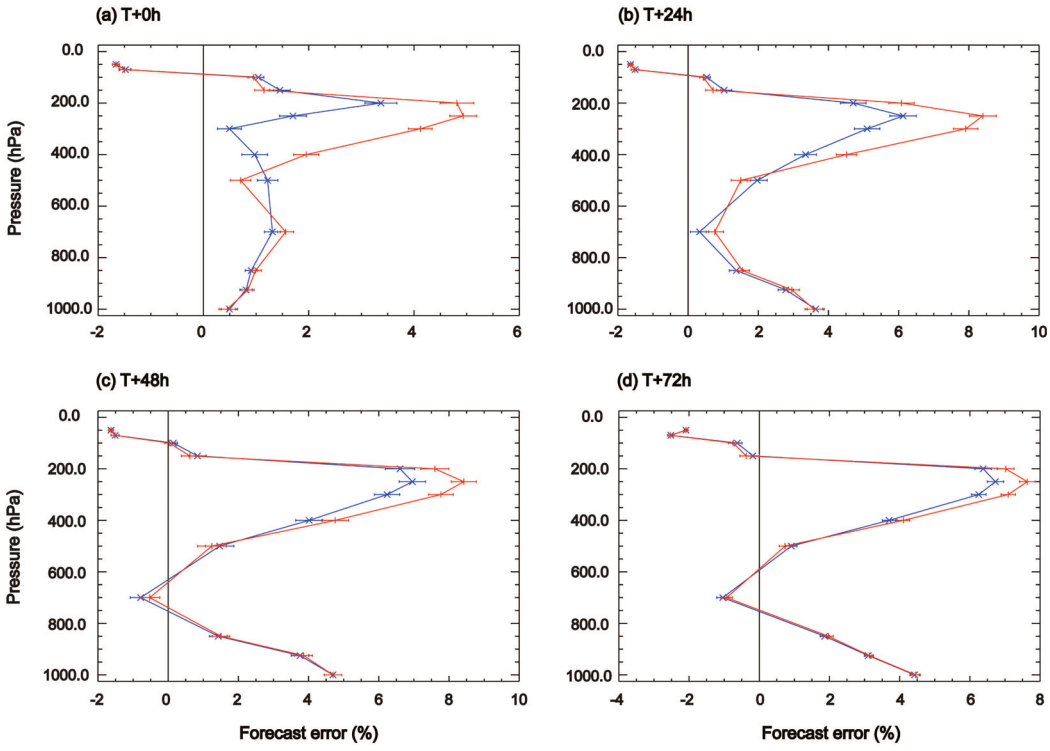

Fig. 14. Vertical structure of the mean bias of relative humidity forecast errors between forecasts and radiosonde observations at the forecast hours of T+0 to T+72. Red and blue lines indicate the control and experiment runs, respectively. Horizontal bars indicate one standard deviation of the uncertainty.

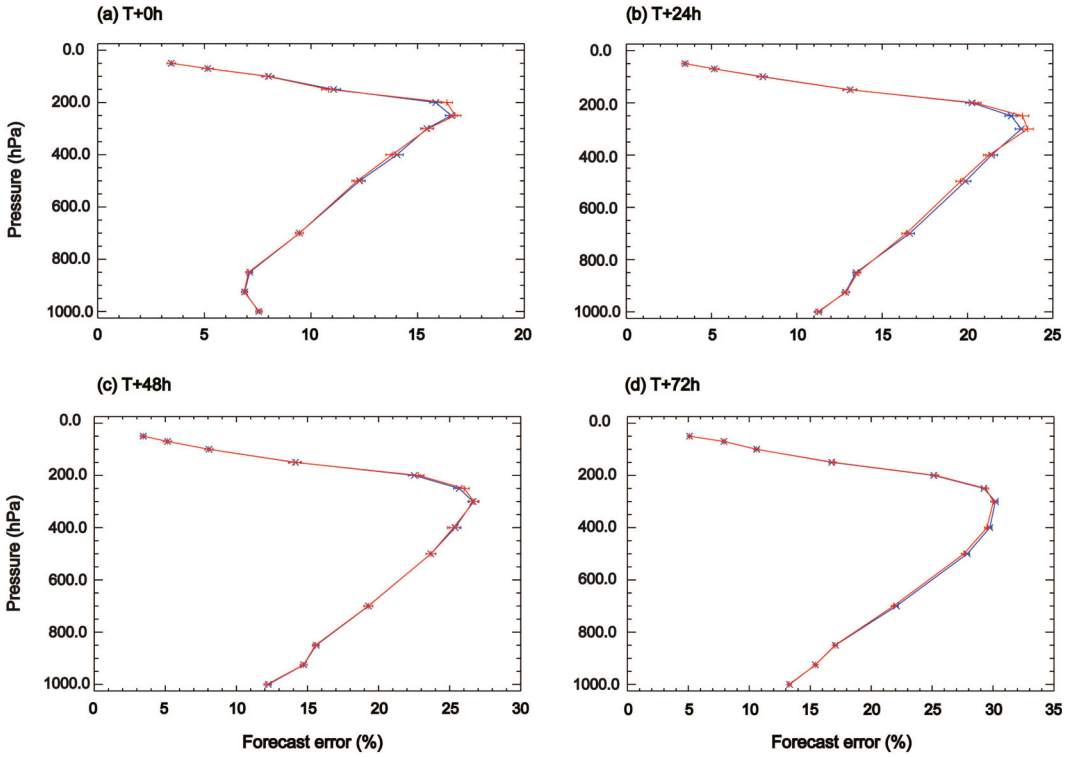

Fig. 15. As in Fig. 14 except for the RMSE of the relative humidity errors.

may be minimal, probably due to the high noise levels in these channels. Thus, the overall improved forecasts for temperature and humidity in the upper troposphere are primarily due to the newly selected H_2O channels.

It is also important to note that the difference in the relative humidity bias in the upper troposphere between the control and experiment runs became smaller with forecasting hour, except around the 250 hPa level at T+72 (Fig. 14). The assimilation of additional channels in the experiment run produces a humidity analysis closer to the radiosonde values. However, such bias reduction disappears quickly and the humidity bias tends to return to the level of the control run.

6. Conclusions and discussion

In this study, we carried out a new IASI channel selection with the aim of improving the performance of UM model forecasts. The method employs a 1D-Var approach with a newly defined figure of merit called the CSI. In this procedure, in order to alleviate the known comparatively large influence of water vapor on the channel selection, a weight obtained by normalizing each layer's mean water vapor with the mean water vapor in the lowest model layer, is given to each layer's water vapor. These weights are only given to the diagonal component of the error covariance matrix because there is no way to give such weights to the cross-covariance components. Also examined is how the CSI compares when the 1D-Var approach is used with a different figure of merit—that of the ER approach. The ER method adopted in this study is different from the Collard (2007) sequential/linear method because of the nonlinear aspect of 1D-Var. However, different from the CSI method, water vapor weights are not given to the error covariance matrix because the ER method requires the full error-covariance matrix.

By applying the CSI method, 200 channels were selected out of the 314 provisional IASI channels. Compared with the operationally used 183 channels at the UKMO for the UM data assimilation system, the new channels share 149 channels, while the other 51 channels are new. Those new channels include H_2O channels representing the water vapor absorption in the middle to upper troposphere, channels in the O_3 absorption band, and channels over the shortwave infrared IASI band 3.

Compared to the CSI results, the ER method with 1D-Var selected fewer channels over the CO_2 absorption band but more channels over the H_2O absorption band. In particular, more upper-tropospheric H_2O channels over 1350–1600 cm^{-1} were selected because contributions of upper-tropospheric H_2O channels to the ER are much larger than for channels in any other spectral band. It seems that the ER method should be applied separately to each important absorption band, combining results subjectively to give the total number of selected channels. Thus, the CSI method is found to be more objective.

To assess the impact of the 189 new channels on the data assimilation system compared to the operationally used channels, an experiment was conducted for a summer period from 4 July to 7 August 2013, using the UKMO global UM system. The O_3 channels were excluded in this experiment because the UM model does not explicitly forecast the O_3 concentra-

tions. While the control run used the 183 UKMO operational IASI channel data, the experiment run used the 189 newly selected channels during the nighttime and 163 channels during the daytime, after removing 26 band 3 channels. Apart from the IASI channels, the same observational data were used for both the control and experiment runs.

In the first-guess departure analysis of the control and experiment runs, a significant difference in the humidity field was found when bias-corrected sounders (i.e., ATOVS, AIRS, and CrIS) measurements and radiosonde observations were compared. The control run showed a small positive humidity bias, while the experiment run showed a negative bias whose absolute magnitude was significantly larger than the positive mean bias shown in the control run.

Results from the first-guess departure analysis of the humidity from radiosonde observations showed a control run with a large moisture bias, compared to the near-zero bias results from sounding sensor measurements. However, the moisture bias was substantially reduced in the experiment run, indicating the positive impact of the new IASI channels on the humidity field. The differences in the first-guess departure of the humidity field between the sounding sensors and radiosonde observations were likely due to the bias correction applied to the radiances measured by the sounding sensors. The global forecasts from the control and experiment runs also demonstrated that the humidity biases in the upper troposphere, shown in the control run, were substantially reduced by the use of the new IASI channels. The improvement in the humidity field was likely due to the use of different H_2O channels, which may better represent the upper-tropospheric humidity.

This study attempted to select optimal channels from the 314 provisional IASI channels that have been operationally received via EUMETCAST in the UM assimilation system. It would have been much more desirable if the selection was made from the total 8461 IASI channels using the proposed CSI method. However, the computational burden caused by1D-Var runs is formidable; even in the case of selecting 200 channels from 314 pre-selected channels, the total number of 1D-Var runs required is 25 740 000 [= $(314 + 313 + 312 + \cdots + 115) \times 600$ profiles]. Being aware of the limitation brought by starting with a small number of pre-selected channels, it is of interest to examine how the channel selection by the CSI method is influenced by a different set of preselected channels. It is of further interest to examine how the new set of channels, if there is any, is comparatively informative against the old set (here, for example, 314 EUMETSAT channels versus 500 channels). As a case in point, we attempted to select new channels from 500 pre-selected EUMETSAT channels (distributed from 15 October 2014) by using the same procedures provided in this paper. The results, given in the Appendix, suggest that it may be necessary to select a new subset of channels if the environment is changed, in association with the NWP model or supply of satellite data, in order to perform more efficient data assimilation. Considering that all channels across the absorption bands should not be equal, determining the most important channels in sequence must be a valuable effort.

One caveat to this study stems from the use of the diagonal component alone from the error covariance matrix to give weights to the water vapor profile and thus to alleviate the strong water vapor contributions to the channel selection. Since IASI channels suitable for the NWP system depend considerably on various factors (e.g., sensor stability, performance of the NWP model, and upgrading of the radiative transfer model), the impact of ignoring the cross covariance should be assessed in the future.

Acknowledgements. This study was carried out through a collaboration between the UKMO and the Korea Meteorological Administration (KMA). This research was supported by the KMA Research and Development Program under Grant No. KMIPA 2015-1060, and was also supported by the BK21 Plus Project of the Korean government.

APPENDIX

Five-hundred EUMETSAT channels comprise 300 channels suggested by Collard (2007), 43 channels chosen by Collard and McNally (2009), 134 channels from Martinet et al. (2014), and 23 monitoring channels. Based on the same CSI selection procedure using 1D-Var taken in this study, the first 220 channels were selected from the 500 EUMETSAT channels because the cumulative CSI tends to level off after 180 (Fig. A1). In other words, additional channels after the first 180 channels have little impact on the cumulative CSI. Therefore, we determined the first 200 channels to be optimal and these are referred to as EUMETSAT 200.

Compared with 200 channels selected from 314 channels (referred to as Collard 200), EUMETSAT 200 includes more split window channels and lower-tropospheric water vapor channels from Martinet's 134 channels and some additional

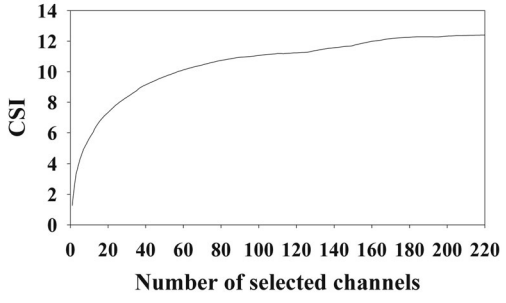

Fig. A1. Relationship between the CSI and the number of selected IASI channels from EUMETSAT 500.

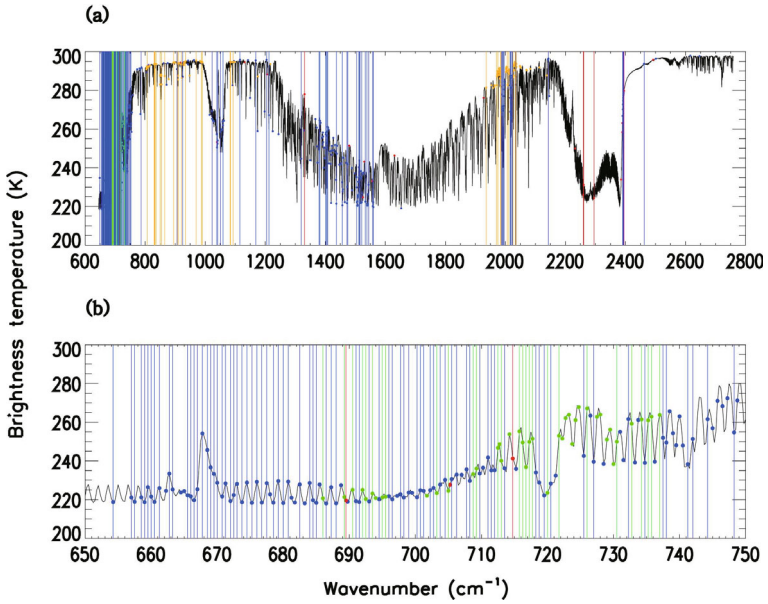

Fig. A2. Spectral distribution of 200 IASI channels selected from EUMETSAT 500 over the (a) infrared band (600–2800 cm^{-1}) and (b) CO_2 absorption band (650–750 cm^{-1}). Vertical lines in color indicate the selected channels, while dots represent channels not in the 200 channels. EUMETSAT's 500 channels consist of Collard's 300 channels (blue), Collard and McNally's 43 channels (green), Martinet's 134 channels (yellow), and 23 monitoring channels (red).

Table A1. Number of selected channels against spectral ranges.

Band	Wavenumber (cm^{-1})	200 from 314 channels	200 from 500 channels
A	600–750	110	112
B	750–1200	32	31
C	1200–2000	32	35
D	2000–2700	26	22
Total		200	200

channels from 43 CO_2 channels of Collard and McNally (2009) (Fig. A2). In spite of those changes in spectral locations, however, the numbers of selected channels in each spectral band appear to be nearly the same (Table A1). This means that some channels of Collard 200 in each spectral band are replaced by channels in Martinet's 134 channels and Collard's 43 channels, but adding/removing little in the given spectral band. Nonetheless, from the perspective of total cumulative CSI, EUMETSAT 200 yields a CSI 6.7% larger than from Collard 200, suggesting that EUMETSAT 200 is more informative than Collard 200.

REFERENCES

Bauer, P., A. Thorpe, and G. Brunet, 2015: The quiet revolution of numerical weather prediction. *Nature*, **525**, 47–55, doi: 10.1038/nature14956.

Bormann, N., and P. Bauer, 2010: Estimates of spatial and interchannel observation-error characteristics for current sounder radiances for numerical weather prediction. I: Methods and application to ATOVS data. *Quart. J. Roy. Meteor. Soc.*, **136**, 1036–1050, doi: 10.1002/qj.616.

Cameron, J. R. N., A. D. Collard, and S. J. English, 2005: Operational use of AIRS observations at the Met Office. *Proceedings of the 14th International TOVS Study Conf.*, Beijing, China.

Collard, A. D., 2007: Selection of IASI channels for use in numerical weather prediction. *Quart. J. Roy. Meteor. Soc.*, **133**, 1977–1991, doi: 10.1002/qj.178.

Collard, A. D., and A. P. McNally, 2009: The assimilation of Infrared Atmospheric Sounding Interferometer radiances at ECMWF. *Quart. J. Roy. Meteor. Soc.*, **135**, 1044–1058, doi: 10.1002/qj.410.

Deblonde, G., J. F. Mahfouf, B. Bilodeau, and D. Anselmo, 2007: One-dimensional variational data assimilation of SSM/I observations in rainy atmospheres at MSC. *Mon. Wea. Rev.*, **135**, 152–172, doi: 10.1175/MWR3265.1.

Dee, D. P., and Coauthors, 2011: The ERA-Interim reanalysis: Configuration and performance of the data assimilation system. *Quart. J. Roy. Meteor. Soc.*, **137**, 553–597, doi: 10.1002/qj.828.

English, S. J., 1999: Estimation of temperature and humidity profile information from microwave radiances over different surface types. *J. Appl. Meteor.*, **38**, 1526–1541, doi: 10.1175/1520-0450(1999)038<1526:EOTAHP>2.0.CO;2.

English, S. J., R. J. Renshaw, P. C. Dibben, A. J. Smith, P. J. Rayer, C. Poulsen, F. W. Saunders, and J. R. Eyre, 2000: A comparison of the impact of TOVS arid ATOVS satellite sounding data on the accuracy of numerical weather forecasts. *Quart. J. Roy. Meteor. Soc.*, **126**, 2911–2931, doi: 10.1002/qj.49712656915.

Gambacorta, A., and C. D. Barnet, 2013: Methodology and information content of the NOAA NESDIS operational channel selection for the Cross-Track Infrared Sounder (CrIS). *IEEE*

Trans. Geosci. Remote Sens., **51**, 3207–3216, doi: 10.1109/TGRS.2012.2220369.

Harris, B. A., and G. Kelly, 2001: A satellite radiance-bias correction scheme for data assimilation. *Quart. J. Roy. Meteor. Soc*., **127**, 1453–1468, doi: 10.1002/qj.49712757418.

Hilton, F., N. C. Atkinson, S. J. English, and J. R. Eyre, 2009: Assimilation of IASI at the Met Office and assessment of its impact through observing system experiments. *Quart. J. Roy. Meteor. Soc*., **135**, 495–505, doi: 10.1002/qj.379.

Joo, S., J. Eyre, and R. Marriott, 2013: The impact of MetOp and other satellite data within the Met Office global NWP system using an adjoint-based sensitivity method. *Mon. Wea. Rev*., **141**, 3331–3342, doi: 10.1175/MWR-D-12-00232.1.

Kelly, G., and J.-N. Thépaut, 2007: Evaluation of the impact of the space component of the global observing system through observing system experiments. *ECMWF Newsletter*, **113**, 16–28.

Lorenc, A. C., and R. T. Marriott, 2014: Forecast sensitivity to observations in the Met Office Global numerical weather prediction system. *Quart. J. Roy. Meteor. Soc*., **140**, 209–224, doi: 10.1002/qj.2122.

Martinet, P., L. Lavanant, N. Fourrié, F. Rabier, and A. Gambacorta, 2014: Evaluation of a revised IASI channel selection for cloudy retrievals with a focus on the Mediterranean basin. *Quart. J. Roy. Meteor. Soc*., **140**, 1563–1577, doi: 10.1002/qj.2239.

Matricardi, M., F. Chevallier, G. Kelly, and J.-N. Thépaut, 2004: An improved general fast radiative transfer model for the assimilation of radiance observations. *Quart. J. Roy. Meteor. Soc*., **130**, 153–173, doi: 10.1256/qj.02.181.

Migliorini, S., 2015: Optimal ensemble-based selection of channels from advanced sounders in the presence of cloud. *Mon. Wea. Rev*., **143**, 3754–3773, doi: 10.1175/MWR-D-14-00249.1.

Parrish, D. F., and J. C. Derber, 1992: The National Meteorological Center's spectral statistical-interpolation analysis system. *Mon. Wea. Rev*., **120**, 1747–1763, doi: 10.1175/1520-0493(1992)120<1747:TNMCSS>2.0.CO;2.

Pavelin, E. G., S. J. English, and J. R. Eyre, 2008: The assimilation of cloud-affected infrared satellite radiances for numerical weather prediction. *Quart. J. Roy. Meteor. Soc*., **134**, 737–749, doi: 10.1002/qj.243.

Rabier, F., N. Fourrié, D. Chafaï, and P. Prunet, 2002: Channel selection methods for Infrared Atmospheric Sounding Interferometer radiances. *Quart. J. Roy. Meteor. Soc*., **128**, 1011–1027, doi: 10.1256/0035900021643638.

Rawlins, F., S. P. Ballard, K. J. Bovis, A. M. Clayton, D. Li, G. W. Inverarity, A. C. Lorenc, and T. J. Payne, 2007: The Met Office global four-dimensional variational data assimilation scheme. *Quart. J. Roy. Meteor. Soc*., **133**, 347–362, doi: 10.1002/qj.32.

Rodgers, C. D., 2000: *Inverse Methods for Atmospheric Sounding*: *Theory and Practice. Series on Atmospheric*, *Oceanic and Planetary Physics*, Vol. 2. World Scientific, 256 pp.

Saunders, R. W., T. A. Blackmore, B. Candy, P. N. Francis, and T. J. Hewison, 2013: Monitoring satellite radiance biases using NWP models. *IEEE Trans. Geosci. Remote Sens*., **51**, 1124–1138, doi: 10.1109/TGRS.2012.2229283.

Siméoni, D., C. Singer, and G. Chalon, 1997: Infrared atmospheric sounding interferometer. *Acta Astronautica*, **40**, 113–118, doi: 10.1016/S0094-5765(97)00098-2.

Smith, F. I., 2014: Improving the information content of IASI assimilation for numerical weather prediction. PhD. dissertation, Department of Physics and Astronomy, University of Leicester.

Weston, P., 2011: Progress towards the implementation of correlated observation errors in 4D-Var. Forecasting Research Tech. Rep. 560, Met Office, Exeter, UK.

Weston, P., E. G. Pavelin, and A. D. Collard, 2013: NWP SAF Met Office 1D-Var User Manual. NWPSAF-MO-UD-006.

Weston, P. P., W. Bell, and J. R. Eyre, 2014: Accounting for correlated error in the assimilation of high-resolution sounder data. *Quart. J. Roy. Meteor. Soc*., **140**, 2420–2429, doi: 10.1002/qj.2306.